RESEARCH

Homogenization in locally resonant anisotropic metamaterials: mode conversion and selective wave polarization

David Faraci[1] · Angela Vincenti[2] · Claudia Comi[1]

Received: 12 December 2025 / Revised: 17 March 2026 / Accepted: 18 March 2026

Abstract
Two-scale homogenization provides an effective tool for the design of microstructured materials. In particular, when considering periodic locally resonant metamaterials with soft inclusions in a stiff matrix, asymptotic homogenization allows for the effective prediction of band gaps in the long wave regime. When inclusions lack rotational symmetry, the resulting homogenized medium is characterized by anisotropic stiffness and anisotropic frequency-dependent mass density, leading to more complex wave propagation behavior. In this work, by means of numerical and analytical examples, we show how the equivalent homogenized formulation is able to correctly reproduce the dispersion and wave transmission properties of the heterogeneous anisotropic medium. The role of the anisotropic equivalent mass tensor to selectively polarize elastic waves and to achieve mode conversion is elucidated in particular.

Keywords Asymptotic homogenization · Locally resonant metamaterials · Anisotropic mass · Band gaps · Wave polarization · Mode conversion

1 Introduction

Locally resonant metamaterials (LRMs) have emerged as a powerful class of architected materials capable of manipulating elastic wave propagation at subwavelength scales. Their dynamic behaviour is characterized by the presence of frequency band gaps induced by internal resonant mechanisms, a concept first highlighted in early seminal works on locally resonant sonic materials [1]. In recent years, LRMs have demonstrated promising potential in several applications, such as vibration isolation, impact mitigation and wave-guiding, extending their relevance across structural engineering, acoustics and mechanical design [2–4].

Whilst many authors study LRMs using lumped-mass models [5] or fully numerical FE-based simulations, particularly when dealing with non-linear behaviours [6], it has been proved that two-scale asymptotic homogenization can be a key theoretical tool to analyse the complex response of LRMs, providing closed-form expressions for the homogenized stiffness and dynamic mass tensors in highly contrasted periodic media [7–9]. When inclusions are sufficiently soft, the effective response captures the resonant behaviour of the microstructure, enabling accurate prediction of dispersion properties in the long-wavelength regime [10]. This class of homogenization-based models has recently been extended to coated-inclusion LRMs [11] and locally resonant metaplates [12], offering a unifying mathematical framework for band gap prediction.

The physical origin of band gaps in LRMs is typically associated with an effective dynamic mass density that becomes negative within specific frequency intervals, inhibiting the propagation of elastic waves [13, 14]. An

Published online: 13 April 2026

important recent trend concerns the deliberate introduction of *anisotropy* in LRMs to unlock additional wave-control functionalities. While the homogenized stiffness tensor is often naturally anisotropic in most periodic systems, the dynamic mass tensor is generally treated as isotropic. However, appropriately designed resonant inclusions—non-symmetric coatings, eccentric cores, shape-engineered cavities or ellipsoidal resonators—can induce anisotropic effective mass density [15, 16]. Such anisotropy leads not only to the modification of existing band gaps but also to polarization-dependent propagation, negative refraction, selective mode conversion and controlled transmission enhancement [17–19]. In particular, when the principal components of the dynamic mass tensor have opposite signs, the material exhibits *polarization bands*, where waves can propagate only if aligned with a specific polarization direction dictated by mass anisotropy. These emerging anisotropy-driven mechanisms have been demonstrated both analytically and numerically in LRMs with lumped models [20], asymmetrically coated [15] or geometrically eccentric inclusions [21].

Building on these advances, the present work investigates wave propagation in anisotropic LRMs comprising a stiff matrix with periodically distributed soft elliptical or eccentric inclusions. In Sect. 2 we formulate the problem and exploit two-scale asymptotic homogenization to derive the anisotropic effective stiffness and dynamic mass tensors. Then, Sect. 3 is be devoted to discuss the dispersion properties of the equivalent homogeneous media with emphasis on the role of the mass anisotropy. In Sect. 4, we analyse the effect of the ellipse eccentricity on the dispersion properties. We further assess the predictive capability of the homogenized formulation by comparing it with full-scale numerical simulations on a finite domain, highlighting also the possibility to exploit polarization bands for manipulating elastic wave polarization. With the aid of an analytical solution, we also discuss how the mass anisotropy allows for mode conversion. The results demonstrate that homogenization not only offers fundamental insight into the role of anisotropic mass density but also provides a computationally efficient tool for the design and optimization of next-generation LRMs. Some conclusions are drawn in Sect. 5.

Notation – Vectors and second-order tensors are indicated with bold letters ($\mathbf{a}$, $\mathbf{b}$,…) while blackboard bold is used for fourth-order tensors ($\mathbb{A}$, $\mathbb{B}$,…). We indicate with $\mathbf{e}_i$ the unit vector of the i-th axis, with δ_{ij} the Kronecker's delta, with $\mathbf{I}$ the second-order identity tensor and with $\mathbb{I}$ the fourth-order symmetric identity tensor. We denote with ϵ the small parameter that governs the asymptotic homogenization analysis. Each field of the heterogeneous periodic medium is indicated in the text with the superscript ϵ, e.g., $\mathbf{u}^\epsilon$ for the real displacement field. Homogenized quantities are indicated with the superscript 0, e.g., $\mathbf{u}^0$ for the homogenized displacement field. We denote by $\mathbf{x}$ the macroscopic position vector in the periodic and homogenized media and by $\mathbf{y}$ the fast variable which accounts for fluctuations of fields within the unit cell. Gradient operators with respect to the variables $\mathbf{x}$ and $\mathbf{y}$ are indicated with $\nabla_\mathbf{x}$ and $\nabla_\mathbf{y}$, respectively. Implicit summation over repeated indices is never assumed.

2 Two-scale asympthotic homogenization

Let us consider a metamaterial, characterized by a two-dimensional periodicity in the $x_1 - x_2$ plane and cylindrical in the x_3-direction, composed by a connected matrix (m) and periodically distributed inclusions (f), see Fig. 1a. The unit cell Y^ϵ of the medium, depicted in Fig. 1b, is a rectangle of sides ℓ_1 and ℓ_2 in which we can distinguish the matrix domain Y_m^ϵ and the inclusion one Y_f^ϵ. In the following, we will assume the scale-separation hypothesis, i.e., that the $\epsilon = \max\{\ell_1, \ell_2\}/L \ll 1$, L being the in-plane size of the considered medium Ω.

The propagation of in-plane elastic waves at a certain angular frequency ω is governed by the Helmholtz equation

$$\nabla_\mathbf{x} \cdot \left(\mathbb{D}^\epsilon : \nabla_\mathbf{x}\mathbf{u}^\epsilon\right) + \rho^\epsilon \omega^2 \mathbf{u}^\epsilon = \mathbf{0} \qquad \text{in } \Omega, \tag{1}$$

where $\mathbf{u}^\epsilon = \mathbf{u}^\epsilon(\mathbf{x})$ is the unknown displacement field of the medium, $\rho^\epsilon = \rho^\epsilon(\mathbf{x})$ is the mass density of the material, and $\mathbb{D}^\epsilon = \mathbb{D}^\epsilon(\mathbf{x})$ is the fourth-order elastic stiffness tensor. Both the density and the stiffness are periodically heterogeneous. For isotropic component materials, the elastic stiffness depends on the Lame's constant

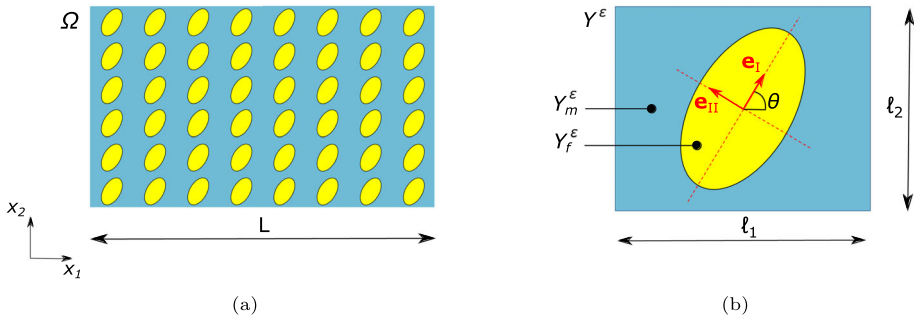

Fig. 1 (a) Metamaterial with periodically distributed elliptic inclusions; (b) close-up view of the unit cell

$\lambda^\epsilon = \lambda^\epsilon(\mathbf{x})$ and $\mu^\epsilon = \mu^\epsilon(\mathbf{x})$ and has the expression

$$\mathbb{D}^\epsilon = 2\mu^\epsilon \mathbb{I} + \lambda^\epsilon \mathbf{I} \otimes \mathbf{I} \quad \text{in } \Omega. \tag{2}$$

To obtain a locally resonant mechanism, we assume the hypothesis of soft inclusions in a stiff matrix. This assumption is introduced in the model by considering a high contrast between the stiffness of the constituent materials, i.e.,

$$\lambda^\epsilon = \begin{cases} \lambda_m & \text{in } Y_m^\epsilon \\ \epsilon^2 \lambda_f & \text{in } Y_f^\epsilon \end{cases}, \quad \mu^\epsilon = \begin{cases} \mu_m & \text{in } Y_m^\epsilon \\ \epsilon^2 \mu_f & \text{in } Y_f^\epsilon \end{cases} \quad \text{and} \quad \rho^\epsilon = \begin{cases} \rho_m & \text{in } Y_m^\epsilon \\ \rho_f & \text{in } Y_f^\epsilon \end{cases}, \tag{3}$$

where λ_m, λ_f are of the same order of magnitude, as well as μ_m, μ_f and ρ_m, ρ_f.

When the wavelength of the propagating wave is by far larger than the unit cell size of the periodic medium, the above-formulated problem can be solved by means of the asymptotic homogenization technique. As discussed in [10], this hypothesis allows the use of homogenization in the low-frequency range, i.e., for

$$\omega \ll \omega_{\max} = \frac{1}{\max\{\ell_1, \ell_2\}} \sqrt{\frac{\mu_m}{\rho_m}}. \tag{4}$$

According to the two-scale asymptotic homogenization [7] we introduce the fast variable $\mathbf{y} = \mathbf{x}/\epsilon$ which lives in the re-scaled unit cell $Y = Y^\epsilon/\epsilon$ of the medium. The solution of (1) is searched in the form

$$\mathbf{u}^\epsilon(\mathbf{x}) = \mathbf{u}^0\left(\mathbf{x}, \frac{\mathbf{x}}{\epsilon}\right) + \epsilon \mathbf{u}^1\left(\mathbf{x}, \frac{\mathbf{x}}{\epsilon}\right) + o(\epsilon) \quad \text{in } \Omega, \tag{5}$$

where the fields $\mathbf{u}^i(\mathbf{x}, \mathbf{y})$ are defined on $\Omega \times Y$ and are $Y-$periodic with respect to the second variable. Replacing the ansatz (5) into equation (1), one obtains a sequence of differential problems associated to each order of the small parameter ϵ.

It is possible to show, see [10] for the full derivation, that the 0−th order displacement has the following form

$$\mathbf{u}^0(\mathbf{x}, \mathbf{y}) = \begin{cases} \mathbf{U}^0(\mathbf{x}) & \text{in } \Omega \times Y_m \\ U_1^0(\mathbf{x}) \boldsymbol{\eta}^1(\mathbf{y}, \omega) + U_2^0(\mathbf{x}) \boldsymbol{\eta}^2(\mathbf{y}, \omega) & \text{in } \Omega \times Y_f \end{cases}, \tag{6}$$

where $\mathbf{U}^0(\mathbf{x})$ is the (unknown) homogenized displacement field of the periodic medium, while the frequency-dependent functions $\boldsymbol{\eta}^i(\mathbf{y}, \omega)$ satisfy the *inclusion cell problem*

$$\begin{cases} \nabla_\mathbf{y} \cdot \left(\mathbb{D}_f : \nabla_\mathbf{y} \boldsymbol{\eta}^i\right) + \rho_f \omega^2 \boldsymbol{\eta}^i = \mathbf{0} & \text{in } Y_f \\ \boldsymbol{\eta}^i = \mathbf{e}_i & \text{on } \partial Y_f \end{cases} \quad \text{for } i \in \{1, 2\}. \tag{7}$$

Problem (7) admits a unique solution if ω does not coincide with an eigenfrequency of the inclusion fixed at its boundary. When ω coincides with one of these eigenfrequencies, and the corresponding eigenmode is orthogonal with respect to $\mathbf{e}_i$, the solution is unique up to an arbitrary multiple of such eigenmode. Otherwise, if the eigenmode is not orthogonal to $\mathbf{e}_i$, problem (7) does not admit solution and thus $U_i^0(\mathbf{x}) = 0$.

The homogenized Helmholtz equation of the periodic medium reads

$$\nabla_{\mathbf{x}} \cdot \left(\mathbb{D}^0 : \nabla_{\mathbf{x}} \mathbf{U}^0\right) + \omega^2 \boldsymbol{\rho}^0(\omega) \cdot \mathbf{U}^0 = \mathbf{0} \qquad \text{in } \Omega, \tag{8}$$

where $\mathbb{D}^0$ and $\boldsymbol{\rho}^0(\omega)$ are respectively the homogenized stiffness and mass density tensor of the medium. The components of the fourth-order effective stiffness are computed, for $i, j, h, k \in \{1, 2\}$, as

$$D^0_{ijhk} = \frac{1}{|Y|} \int_{Y_m} \left(\mathbf{e}_i \otimes \mathbf{e}_j + \nabla_{\mathbf{y}} \boldsymbol{\chi}^{ij}\right) : \mathbb{D}_m : \left(\mathbf{e}_h \otimes \mathbf{e}_k + \nabla_{\mathbf{y}} \boldsymbol{\chi}^{hk}\right) \, d\mathbf{y}. \tag{9}$$

The field $\boldsymbol{\chi}^{ij}(\mathbf{y})$ in (9), with $i, j \in \{1, 2\}$, is the displacement of the matrix, subject to a uniform eigenstrain $\mathbf{e}_i \odot \mathbf{e}_j = (\mathbf{e}_i \otimes \mathbf{e}_j + \mathbf{e}_j \otimes \mathbf{e}_i)/2$, with periodic boundary conditions and with a void instead of the inclusion. It is obtained, up to a rigid translation, as the solution of the following *matrix cell problem*

$$\begin{cases} \nabla_{\mathbf{y}} \cdot \left[\mathbb{D}_m : \left(\mathbf{e}_i \otimes \mathbf{e}_j + \nabla_{\mathbf{y}} \boldsymbol{\chi}^{ij}\right)\right] = \mathbf{0} & \text{in } Y_m \\ \boldsymbol{\chi}^{ij} \text{ periodic} & \text{on } \partial Y \\ \left[\mathbb{D}_m : \left(\mathbf{e}_i \otimes \mathbf{e}_j + \nabla_{\mathbf{y}} \boldsymbol{\chi}^{ij}\right)\right] \cdot \mathbf{n} \text{ anti-periodic} & \text{on } \partial Y \\ \left[\mathbb{D}_m : \left(\mathbf{e}_i \otimes \mathbf{e}_j + \nabla_{\mathbf{y}} \boldsymbol{\chi}^{ij}\right)\right] \cdot \mathbf{n} = \mathbf{0} & \text{on } \partial Y_m \setminus \partial Y \end{cases}, \tag{10}$$

where $\mathbf{n}$ is the outward normal at the boundary. Hence $\mathbb{D}^0$, whose entries are defined by equation (9), represents the effective stiffness of the metamaterial when inclusions are replaced by voids.

The effective mass $\boldsymbol{\rho}^0(\omega)$ of the medium, in (8), turns out to be a frequency-dependent second-order tensor, whose components are given by

$$\rho^0_{ij}(\omega) = \rho_m \frac{|Y_m|}{|Y|} \delta_{ij} + \frac{\rho_f}{|Y|} \int_{Y_f} \eta^i_j(\mathbf{y}, \omega) \, d\mathbf{y}. \tag{11}$$

Considering the variational formulations of problems (7) and (10), it is possible to show that $\mathbb{D}^0$ possesses minor and major symmetries and satisfies the strong ellipticity condition, while $\boldsymbol{\rho}^0(\omega)$ is symmetric.

3 Band gaps and polarization bands

The homogenized medium provided by the asymptotic homogenization, governed by equation (8), is characterized by an anisotropic stiffness tensor and also by an anisotropic frequency-dependent mass density tensor. The latter is real, symmetric and, for the spectral theorem, admits the following representation

$$\boldsymbol{\rho}^0(\omega) = \rho^0_{\mathrm{I}}(\omega) \, \mathbf{e}_{\mathrm{I}} \otimes \mathbf{e}_{\mathrm{I}} + \rho^0_{\mathrm{II}}(\omega) \, \mathbf{e}_{\mathrm{II}} \otimes \mathbf{e}_{\mathrm{II}}, \tag{12}$$

where $\rho^0_{\mathrm{I}}(\omega)$, $\rho^0_{\mathrm{II}}(\omega)$ are the (real) principal mass densities and $\mathbf{e}_{\mathrm{I}}$, $\mathbf{e}_{\mathrm{II}}$ are the corresponding (orthogonal) principal mass directions.

The dispersion properties of the effective equivalent medium can be obtained by considering the plane wave

$$\mathbf{U}^0(\mathbf{x}) = \mathbf{p} e^{-\mathrm{i}\mathbf{k}\cdot\mathbf{x}} \qquad \text{in } \Omega, \tag{13}$$

Table 1 Material properties

material	λ [MPa]	μ [MPa]	ρ [kg/m^3]
aluminium	51000	26000	2500
PVC	140	36	1500

where $\mathbf{p}$ is the polarization vector and $\mathbf{k} = k\mathbf{n}$ is the wavevector, k being the wavenumber and $\mathbf{n}$ the direction of propagation. Replacing (13) into (8), one obtains the homogenized dispersion relation

$$\left(\mathbf{Q}^0(\mathbf{n}) - c^2\boldsymbol{\rho}^0(\omega)\right)\cdot\mathbf{p} = \mathbf{0}, \tag{14}$$

where $\mathbf{Q}^0(\mathbf{n}) = \mathbf{n}\cdot\mathbb{D}^0\cdot\mathbf{n}$ is the homogenized acoustic tensor, which is positive definite, and $c = \omega/k$ is the wave velocity. The non-standard eigenvalue problem (14) defines two real eigenvalues c_α^2, c_β^2 associated to the corresponding eigenvectors $\mathbf{p}_\alpha, \mathbf{p}_\beta \neq \mathbf{0}$ which, in general, do not coincide with $\mathbf{e}_\mathrm{I}, \mathbf{e}_\mathrm{II}$ and are not orthogonal. The two eigenvalues can be expressed by the Rayleigh ratios

$$c_\alpha^2 = \frac{\mathbf{p}_\alpha\cdot\mathbf{Q}^0\cdot\mathbf{p}_\alpha}{\mathbf{p}_\alpha\cdot\boldsymbol{\rho}^0\cdot\mathbf{p}_\alpha} \quad \text{and} \quad c_\beta^2 = \frac{\mathbf{p}_\beta\cdot\mathbf{Q}^0\cdot\mathbf{p}_\beta}{\mathbf{p}_\beta\cdot\boldsymbol{\rho}^0\cdot\mathbf{p}_\beta}. \tag{15}$$

Since $\mathbf{Q}^0$ is positive definite, the numerators in (15) are always positive. Thus, the sign of c_α^2 and c_β^2, depends on the sign of the quadratic form defined by $\boldsymbol{\rho}^0$. As we discussed in [21, 22], three possible cases arise for two-dimensional locally-resonant metamaterials:

① $\boldsymbol{\rho}^0(\omega)$ is positive definite, hence the denominators of (15) are positive. Two real wave velocities c_α, c_β exist and elastic waves can propagate, the corresponding eigenvectors $\mathbf{p}_\alpha, \mathbf{p}_\beta$ give the polarization of such waves (*pass band*);

② $\boldsymbol{\rho}^0(\omega)$ is negative definite, hence the denominators of (15) are negative. Both wave velocities c_α and c_β become imaginary, therefore only evanescent waves exist, which are spatially attenuated (*band gaps*);

③ $\boldsymbol{\rho}^0(\omega)$ is indefinite (ρ_I^0 and ρ_II^0 have different sign). As we demonstrated in [21], only one of the two denominators in (15) is positive in such a case. Without loss of generality, let us assume that the one related to c_α^2 is positive. This implies that only c_α is real-valued, and elastic waves polarized as $\mathbf{p}_\alpha$ can propagate without being attenuated. Waves polarized as $\mathbf{p}_\beta$, conversely, are damped out since c_β is imaginary. In such frequency intervals, elastic waves are selectively polarized by the metamaterial (*polarization bands*).

The periodic repetition of elliptic inclusions, as in Fig. 1, represents a simple case that allows the formation of polarization bands in locally-resonant binary metamaterial. The principal directions of mass are aligned with the ellipse symmetry axes (dashed in red in the same figure). We will use $\mathbf{e}_\mathrm{I}$ to indicate the principal direction along the major axis, forming an angle θ with respect to the x_1 direction, and $\mathbf{e}_\mathrm{II}$ for the one aligned with the minor axis of the ellipse. The eccentricity of the ellipse is indicated with $e = \sqrt{a^2 - b^2}/a$, where a and b are, respectively, the major and minor semi-axes lengths.

To illustrate the effect of the anisotropy of the equivalent mass density, we consider a metamaterial with an aluminium matrix and elliptic polyvinyl chloride (PVC) inclusions. The properties of the constituent materials, listed in Table 1, satisfy the high stiffness contrast hypothesis assumed in Section 2. The unit cell is assumed to be square ($\ell_1 = \ell_2 = \ell$) with a horizontal ($\theta = 0$) elliptical inclusion of area $|Y_f| = \ell^2/2$ and eccentricity $e = 0.5$. The effective mass tensor of the medium is obtained through (11) by solving the inclusion cell problems (7). In this case, where $\mathbf{e}_\mathrm{I} = \mathbf{e}_1$ and $\mathbf{e}_\mathrm{II} = \mathbf{e}_2$, we have that $\rho_{11}^0 = \rho_\mathrm{I}^0$, $\rho_{22}^0 = \rho_\mathrm{II}^0$ and $\rho_{12}^0 = 0$.

Figure 2a shows the principal mass densities, as a function of the natural frequency $f = \omega/2\pi$, in the range $0.9 \div 1.2\, f_0$ where f_0 is the second eigenfrequency of a circular inclusion fixed at its boundary and having the same area of the ellipse. The homogenized mass density is normalized with the static effective mass of the medium,

 https://doi.org/10.1007/s11012-026-02111-9

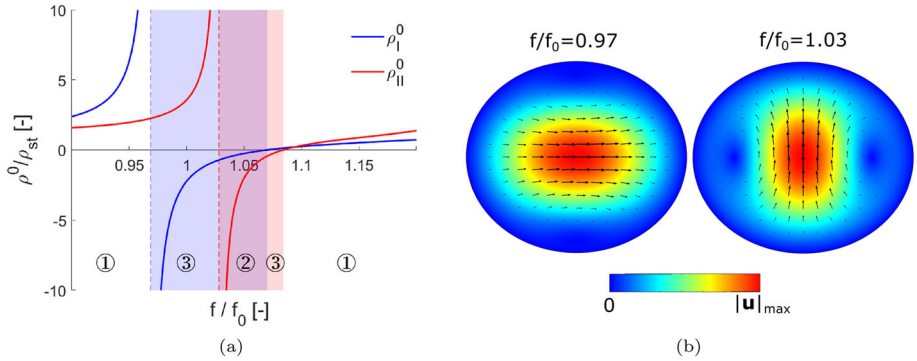

Fig. 2 (a) Homogenized principal mass densities versus frequency for $\ell_1 = \ell_2 = \ell$, $|Y_f| = \ell^2$ and $e = 0.5$. (b) Contour of the displacement magnitude for the second and third eigenmodes of the inclusion fixed at its boundary

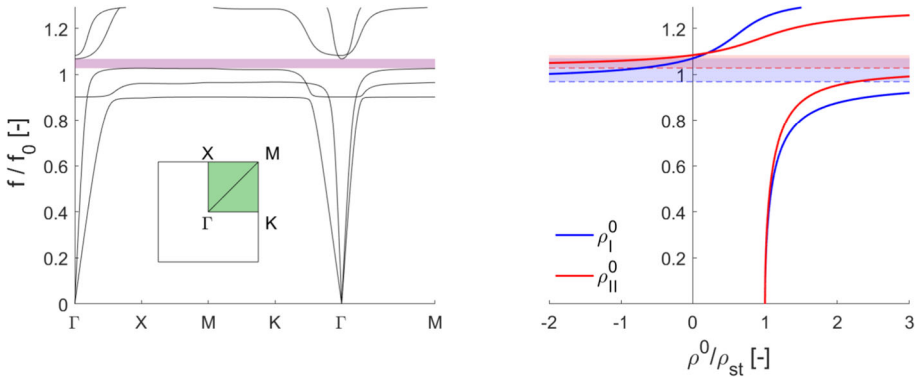

Fig. 3 Comparison between the band gap computed through Bloch-Floquet analysis (left) and the one predicted through homogenization (right), for the case $\ell_1 = \ell_2 = \ell$, $|Y_f| = \ell^2/2$, $e = 0.5$ and $\theta = 0$

defined as

$$\rho_{st} = \rho_m \frac{|Y_m|}{|Y|} + \rho_f \frac{|Y_f|}{|Y|}. \tag{16}$$

Both principal masses ρ^0_{I} (blue curve) and ρ^0_{II} (red curve) have a piece-wise monotonously increasing behavior and have, respectively, a vertical asymptote at $f/f_0 = 0.97$ and $f/f_0 = 1.03$. These are the second and the third eigenfrequency of the elliptical inclusion fixed at its boundary, whose eigenmodes are depicted in Fig. 2b with the contour of the displacement magnitude. In the same figure, black arrows indicate the direction of the displacement field. The vibration mode at $f/f_0 = 0.97$ is orthogonal with respect to $\mathbf{e}_{\mathrm{II}}$ but not with respect to $\mathbf{e}_{\mathrm{I}}$. This is the reason why only ρ^0_{I} has a vertical asymptote for $f/f_0 = 0.97$. Similarly, since the eigenmode associated to $f/f_0 = 1.03$ is orthogonal to $\mathbf{e}_{\mathrm{I}}$ only, ρ^0_{II} is the principal mass that diverges at the corresponding eigenfrequency.

The presence of vertical asymptotes, see Figure 2a, implies the presence of intervals where only p^0_I is negative (shaded in blue), only $p^0_I I$ is negative (shaded in red) or where both the principal masses are negative (shaded in purple). These regions have been marked on the plot with the corresponding number identifying the different cases discussed above of propagation properties in the equivalent medium.

To validate the band gap prediction provided by asymptotic homogenization, which from Fig. 2a occurs from $1.03\,f_0$ to $1.07\,f_0$, we perform a Bloch-Floquet analysis on the unit cell of the periodic medium.

The first Brillouin zone of the periodic media is a square of side $2\pi/\ell$ and it is depicted in Fig. 3 on the left. Since the unit cell with horizontal elliptical inclusion possesses only horizontal and vertical symmetry, the irreducible Brillouin zone is the square of vertices Γ, X, M, K, highlighted in green, having side π/ℓ.

The dispersion curves computed numerically are plotted along the path $\Gamma - X - M - K - \Gamma - M$ and the band gap of the metamaterial is shaded in purple. In the same figure, on the right, the (rotated) plot of the homogenized principal mass densities is reported for the sake of comparison. Asymptotic homogenization estimates the opening and closing frequencies of the band gap with a relative error lower than 0.2%, showing the effectiveness of the proposed approach.

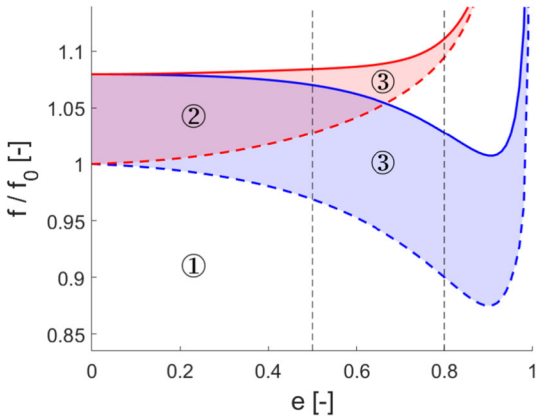

Fig. 4 Intervals of negative ρ_{I}^0 (blue) and ρ_{II}^0 (red) as a function of ellipse eccentricity for $|Y_f| = |Y|/2$

It is worth noticing that all the reasonings conducted in this section and those in the following one are performed within the frequency range of validity of homogenization. In fact, we are dealing with frequencies lower than the maximum one provided by (4), which reads $f_{\max} = \omega_{\max}/2\pi = 1.95\, f_0$.

4 Results

4.1 The eccentricity effect on the dispersion properties

To investigate the role of the eccentricity e of the ellipse, we perform a parametric study by considering a unit cell containing a horizontal elliptic inclusion ($\theta = 0$) with constant filling ratio $|Y_f|/|Y| = 1/2$. Note that the actual shape of the unit cell (square, rectangle, parallelogram) does not intervene in the definition of the effective mass, as the matrix only intervenes through $|Y_m|$ in the filling ratio. Therefore, this parametric study is representative of different metamaterial geometries, provided the cell could strictly contain the elliptic inclusion of given eccentricity.

Figure 4 shows how the frequency intervals in which $\rho_{\mathrm{I}}^0 < 0$ (shaded in blue) and $\rho_{\mathrm{II}}^0 < 0$ (shaded in red) vary as a function of the ellipse eccentricity. Blue and red dashed curves represent the frequency at which the corresponding principal mass density has the vertical asymptote, while the solid ones refer to its zero value. The different regions of the plot are numbered consistently with the cases discussed in Sect. 3 regarding the dispersion properties of the medium.

In particular, it can be observed that for $e = 0$, i.e. when the ellipse becomes a circle, the principal masses ρ_{I}^0 and ρ_{II}^0 become equal and only one band gap can be observed in the spectrum. As the eccentricity of the inclusion increases, the band gap obtained by the superposition of the blue and red shaded regions becomes narrower until it disappears for $e \simeq 0.67$, while polarization bands can be observed as an effect of the mass anisotropy. The dashed vertical lines correspond to the eccentricities $e = 0.5$ and $e = 0.8$ used in the following examples.

4.2 Polarization bands in a finite panel

Let us consider a finite metamaterial panel, such as the one shown in Fig. 5a, made of 30×60 square unit cells of side ℓ, with elliptical inclusions of area $Y_f = \ell^2/2$, eccentricity $e = 0.8$, inclined at $\theta = 45°$. In this case, the principal mass directions $\mathbf{e}_{\mathrm{I}}$ and $\mathbf{e}_{\mathrm{II}}$ are inclined at $+45°$ and $-45°$, respectively. Note that, up to a rigid rotation, this metamaterial is included in the preceding parametric study and the polarization bands can be seen in Fig. 4 for $e = 0.8$.

On the central portion of the left side of the panel, of length 4ℓ, we apply a prescribed horizontal displacement $u_1 = U$ at a given frequency ω, while on the remaining portion of the boundary we prescribe low-reflection boundary conditions.

The numerical solution of the problem is carried out with the commercial finite element software COMSOL Multiphysics. To assess the effectiveness of the homogenization technique to simulate wave propagation in meta-

 https://doi.org/10.1007/s11012-026-02111-9

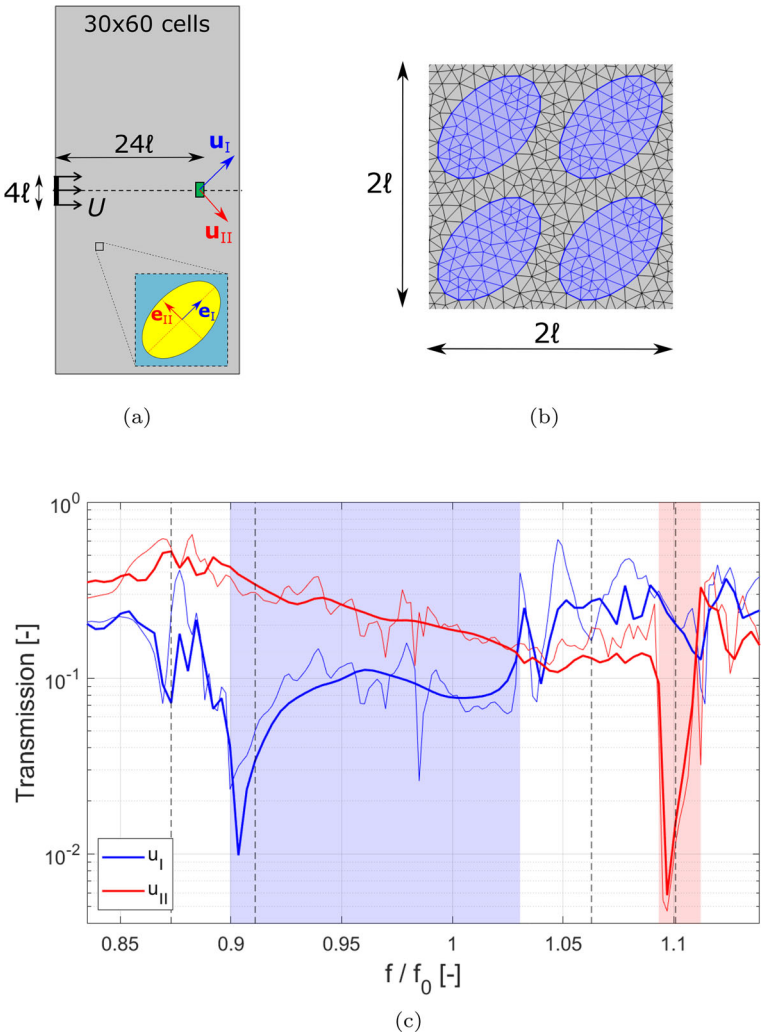

Fig. 5 (a) Geometry of the problem; (b) detail of finite element discretization; (c) transmission of $|u_{\mathrm{I}}|/U$ (blue) and $|u_{\mathrm{II}}|/U$ (red) against frequency for the real (thin lines) and the homogenized (thick lines) solution

materials, we also numerically solve the homogenized problem, eq.(8), replacing the metamaterial by the equivalent anisotropic medium. The fully periodic heterogeneous media has been discretized by 315,000 quadratic serendipity triangular finite elements ($\sim$ 1,260,000 d.o.f). Figure 5b shows the detail of the mesh employed in the analysis on a region of 2×2 unit cells (inclusions are highlighted in blue). The homogenized medium has been instead discretized by 7200 quadratic serendipity quadrilateral elements only ($\sim$ 70, 000 d.o.f). This discretization, which allows to reduce the computational time of 90%, already gives converged results, as verified by using a finer mesh.

Figure 5c shows the comparison between the two solutions in terms of the transmission of the displacement components $|u_{\mathrm{I}}|/U$ (blue curves) and $|u_{\mathrm{II}}|/U$ (red curves) along the principal mass directions as a function of the normalized frequency. The transmission in the actual heterogeneous panel is plotted in thin lines, while the thicker ones refer to the homogenized solution. On the same figure, the intervals in which $\rho^0_{\mathrm{I}} < 0$ ($0.9 \div 1.03\, f_0$ in blue) and $\rho^0_{\mathrm{II}} < 0$ ($1.09 \div 1.11\, f_0$ in red) are shaded. Note that, in the case $e = 0.8$, the intervals of negative principal masses are separated and no band gap is present in the spectrum (see Fig. 4).

There is a qualitatively good agreement between the real and the homogenized transmissions. In particular, it can be observed that at the opening of the blue polarization band, where $\rho^0_{\mathrm{I}} < 0$, the displacement is mainly polarized at $-45°$, i.e., in the direction of the positive principal mass. As commented in Sect. 2 regarding the solvability of (7), this is due to the fact that, since the eigenmode of the fixed inclusion occurring at $f/f_0 = 0.9$ is not orthogonal to $\mathbf{e}_{\mathrm{I}}$, it must be $U^0_{\mathrm{I}} = 0$ for $f/f_0 = 0.9$. A similar reasoning can be applied at the opening of the red polarization band, where waves are mainly polarized at $+45°$.

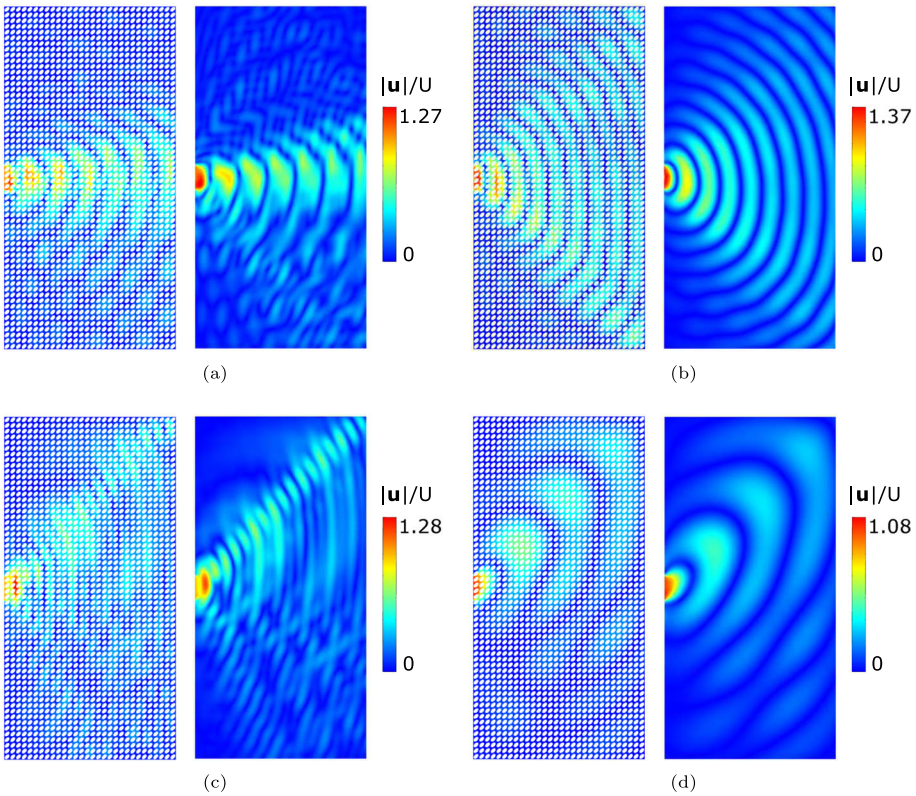

Fig. 6 Contours of $|\mathbf{u}|/U$ for the fully-resolved (left) and homogenized (right) solution for: (a) $f/f_0 = 0.87$, (b) $f/f_0 = 0.91$, (c) $f/f_0 = 1.06$ and (d) $f/f_0 = 1.10$

The two solutions are also compared in terms of the matrix displacement magnitude $|\mathbf{u}|/U$ over the whole domain. Figure 6 shows such comparison for different frequencies belonging to pass bands and polarization bands. The latter are marked in Fig. 5c with dashed black lines. Since the imposed displacement is applied to a small portion of the left boundary of the panel, almost circular wave fronts would occur in an isotropic medium, but, due to stiffness and mass anisotropy, the fronts are distorted.

For the frequencies $f/f_0 = 0.87$ (Fig. 6a) and $f/f_0 = 1.06$ (Fig. 6c), which belong to pass bands, two different wavelengths can be recognized in the contour, as the solution is the superposition of two waves with different polarization vectors and velocities. In contrast, when looking at the frequencies $f/f_0 = 0.91$ (Fig. 6b) and $f/f_0 = 1.10$ (Fig. 6d), only a single wavelength can be observed. This is the effect of polarization bands, where only a single wave with a certain polarization and velocity is allowed to propagate without attenuation.

From the comparison shown in Fig. 6, one can conclude that, in the present case, asymptotic homogenization provides a satisfactory prediction of the solution, showing its ability to deal with different scenarios of elastic wave propagation in anisotropic locally-resonant metamaterials. The example hence validates the asymptotic homogenization approach here developed in the hypothesis of high stiffness contrast between matrix and inclusions. However, the solution of the fully heterogeneous periodic medium converges towards the homogenized one only as $\epsilon = \ell/L \to 0$. No estimation of the relative error, in general, is available a priori for a given $\ell/L \neq 0$.

The polarization effect can be observed in Fig. 7, which displays the contours of the displacement components u_{I}/U and u_{II}/U along the principal directions of mass.

At a frequency that belongs to a pass band, e.g. $f/f_0 = 0.87$ shown in Fig. 7a or $f/f_0 = 1.06$ in Fig. 7c, both displacement components propagate in the medium. Close to the opening of the blue polarization band at $f/f_0 = 0.91$, where $\rho_{\mathrm{I}}^0 < 0$, Fig. 7b clearly shows that the displacement along the direction of negative mass is attenuated and thus $u_{\mathrm{II}} \gg u_{\mathrm{I}}$. Similarly, at $f/f_0 = 1.10$ (Fig. 7d), which is close to the opening of the red polarization band, the wave is almost polarized along $\mathbf{e}_{\mathrm{I}}$.

 https://doi.org/10.1007/s11012-026-02111-9

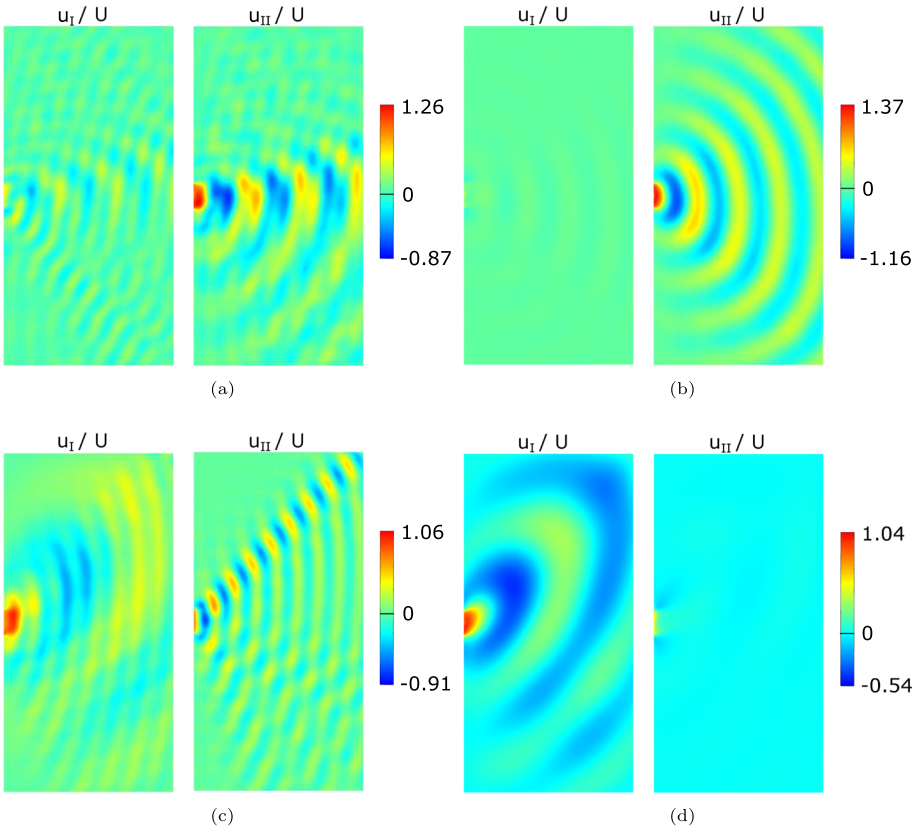

Fig. 7 Contours of u_{I}/U and u_{II}/U for the homogenized solution for: (a) $f/f_0 = 0.87$, (b) $f/f_0 = 0.91$, (c) $f/f_0 = 1.06$ and (d) $f/f_0 = 1.10$

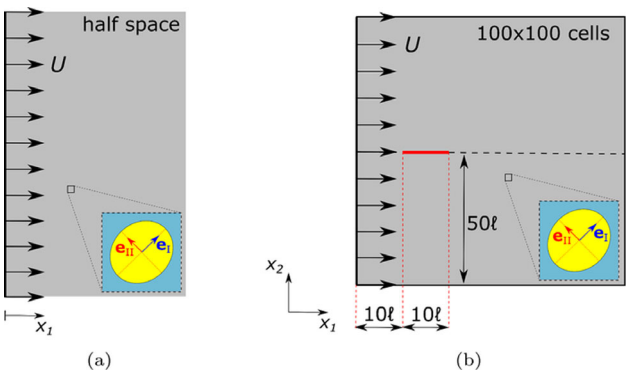

Fig. 8 Geometry of (a) the idealized problem in the half-space and (b) the finite one solved numerically

4.3 Mode conversion

The presence of polarization bands entails the possibility of achieving a mode conversion mechanism for elastic waves, with many potential applications. To highlight this effect, we consider the ideal homogenized problem, depicted in Fig. 8a, of a half-space $x_1 \geq 0$ that has the same properties of the metamaterial having square unit cell of side ℓ with elliptical inclusion of area $|Y_f| = \ell^2/2$, eccentricity $e = 0.5$, and inclined at $\theta = 45°$. To produce a longitudinal wave, we impose a horizontal displacement U, at a given frequency ω, on the boundary $x_1 = 0$. In this way, a plane wave propagating along $\mathbf{e}_1$ is generated.

The homogenized stiffness $\mathbb{D}^0$ is computed through equation (9) by solving the matrix cell problems (10). The effective mass tensor $\boldsymbol{\rho}^0(\omega)$ has principal directions $\mathbf{e}_{\mathrm{I}}$ and $\mathbf{e}_{\mathrm{II}}$ rotated of 45° with respect to $x_1 - x_2$, while the principal masses are those already shown in Fig. 2a.

At each frequency, the non-standard eigenvalue problem (14) can be solved for $\mathbf{n} = \mathbf{e}_1$ to compute the polarization vectors $\mathbf{p}_\alpha(\omega)$, $\mathbf{p}_\beta(\omega)$ and the corresponding (real or imaginary) wave velocities $c_\alpha(\omega)$, $c_\beta(\omega)$. Figure 9a represents the variation of c_α^2 (in blue) and c_β^2 (in red) with the frequency. Velocities are normalized with respect

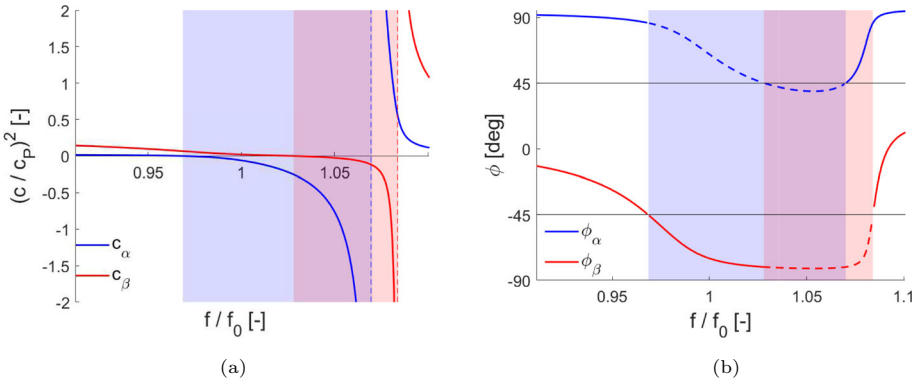

Fig. 9 Frequency dependence of (a) wave velocities and (b) polarization directions for a $\mathbf{e}_1-$propagating wave in the case $|Y_f| = \ell^2/2$, $e = 0.5$ and $\theta = 45°$

to the speed of propagation of pressure waves in the matrix

$$c_P = \sqrt{\frac{\lambda_m + 2\mu_m}{\rho_m}}. \tag{17}$$

Note that, as expected, the wave velocity vanishes when the corresponding principal mass has a vertical asymptote and vice-versa, cp. Figures 9a and 2a.

For each frequency, Fig. 9b shows the angles ϕ_α (in blue) and ϕ_β (in red) that the directions individuated by $\mathbf{p}_\alpha$ and $\mathbf{p}_\beta$ (respectively) form with the positive direction of x_1 for a horizontal propagating wave. Solid lines refer to the polarization associated with a propagating wave, i.e., with $c^2 > 0$, while dashed ones refer to evanescent waves ($c^2 < 0$). At the opening of the blue polarization band ($f/f_0 = 0.97$), the propagating wave is polarized at $\phi_\beta = -45°$, i.e., as the direction of positive mass $\mathbf{e}_{\mathrm{II}}$. Similarly, at the opening of the red polarization band, the propagating wave is polarized along $\mathbf{e}_{\mathrm{I}}$ at $\phi_\alpha = +45°$.

Note that in both polarization bands in Fig. 1b, the propagating wave has a polarization $|\phi| \geq 45°$ which tends to the vertical direction as the band closes. This means that even if a longitudinal wave, with horizontal displacement only, is imposed at the boundary, the displacement tends to become vertical due to the polarization. This allows us to achieve a mode conversion from a longitudinal wave to a shear one.

The solution of the idealized problem set in Fig. 8a on the homogenized half space can be analytically computed. The solution at a frequency ω does not depend on x_2 and reads

$$\mathbf{U}^0(x_1) = A_\alpha \mathbf{p}_\alpha e^{-\mathrm{i}\omega x_1/c_\alpha} + A_\beta \mathbf{p}_\beta e^{-\mathrm{i}\omega x_1/c_\beta} \qquad \text{for } x_1 \geq 0. \tag{18}$$

The coefficients A_α, A_β must be determined from boundary conditions, which for this problem are a horizontal imposed displacement U and zero shear stress at $x_1 = 0$, i.e.,

$$\begin{cases} U_1^0 = U \\ \sigma_{12}^0 = D_{1112}^0 \dfrac{\partial U_1^0}{\partial x_1} + D_{1212}^0 \dfrac{\partial U_2^0}{\partial x_1} = 0 \end{cases} \qquad \text{for } x_1 = 0. \tag{19}$$

Replacing (18) into (19) one obtains

$$\begin{aligned} A_\alpha &= \frac{c_\alpha (D_{1112}^0 p_{\beta 1} + D_{1212}^0 p_{\beta 2})}{c_\alpha p_{\alpha_1} (D_{1112}^0 p_{\beta 1} + D_{1212}^0 p_{\beta 2}) - c_\beta p_{\beta 1} (D_{1112}^0 p_{\alpha 1} + D_{1212}^0 p_{\alpha 2})} U, \\ A_\beta &= -\frac{c_\beta (D_{1112}^0 p_{\alpha 1} + D_{1212}^0 p_{\alpha 2})}{c_\alpha p_{\alpha_1} (D_{1112}^0 p_{\beta 1} + D_{1212}^0 p_{\beta 2}) - c_\beta p_{\beta 1} (D_{1112}^0 p_{\alpha 1} + D_{1212}^0 p_{\alpha 2})} U, \end{aligned} \tag{20}$$

 https://doi.org/10.1007/s11012-026-02111-9

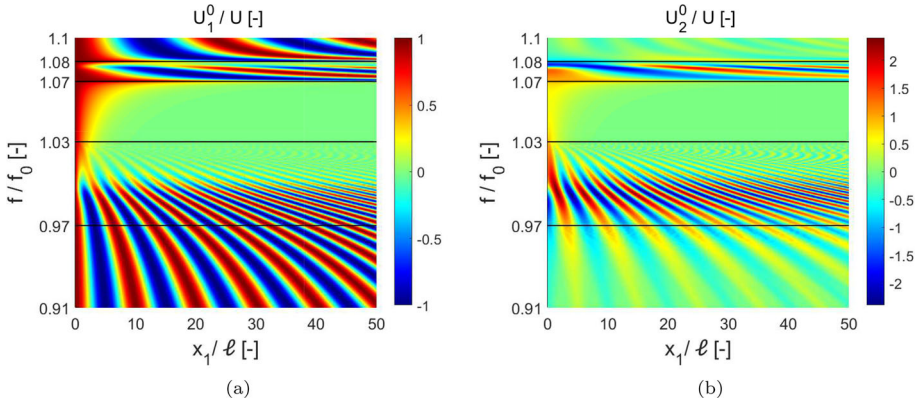

Fig. 10 Contour of: (a) horizontal and (b) vertical displacement field as a function of space and frequency from the solution of the idealized problem

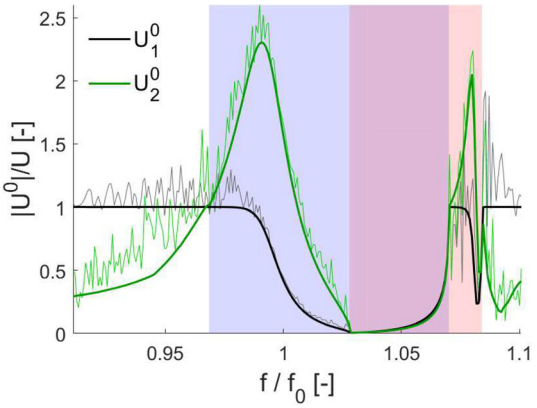

Fig. 11 Maximum magnitude of $|U_1^0|$ (black) and $|U_2^0|$ (green) in the interval $10 \leq x_1/\ell \leq 20$ for the idealized problem (thick lines) and the numerical one (thin, lighter lines)

where $p_{\alpha 1}$, $p_{\beta 1}$ and $p_{\alpha 2}$, $p_{\beta 2}$ are, respectively, the horizontal and vertical components of $\mathbf{p}_\alpha$ and $\mathbf{p}_\beta$. Note that, since polarization vectors and wave velocities depend on frequency, the coefficients (20) depend on frequency as well.

Figure 10a and Fig. 10b show, respectively, the contour of the horizontal and vertical components of the homogenized displacement field given by (18) in the frequency interval $0.91\, f_0 \div 1.1\, f_0$ as a function of the spatial coordinate x_1. Note that the two contours have different color scales. Horizontal black lines separate the different bands that characterize the dispersion properties of the medium.

In the band gap ($1.03 \div 1.07\, f_0$), both displacement components are spatially damped out. In particular, one can observe how the wave attenuation is faster at the opening and decreases as the frequency increases. In the two pass bands considered ($0.91 \div 0.97\, f_0$ and $1.08 \div 1.1\, f_0$), the amplitude of the horizontal displacement (equal to the imposed one U) is greater than the vertical one. Vice versa, in polarization bands ($0.97 \div 1.03$ and $1.07 \div 1.08$), the amplitude of U_2^0 is higher than U_1^0, thus achieving the conversion of the longitudinal wave into a coupled longitudinal-shear wave. A similar effect was obtained e.g. in [23, 24] considering perforated media with elliptic holes.

This can also be visualized by looking at the maximum displacement magnitudes $|U_1^0|$ and $|U_2^0|$, in a region sufficiently far away from the boundary ($x_1/\ell \geq 10$), as shown in Fig. 11. The maximum amplitude of the horizontal displacement (black thick curve) is equal to U in pass bands, decreases in polarization bands and reaches zero value at the opening of the band gap. Conversely, the amplitude of the vertical component (green thick curve) is lower than the horizontal one in the pass bands, but becomes greater in the polarization bands of the metamaterial.

To validate this analytical result, we numerically compute the solution of the problem in a finite-size domain. Figure 8b depicts the square region of side 100ℓ modeled as the homogenized medium of the same metamaterial considered in the idealized problem. On the left edge, we impose a horizontal displacement U, while on the other three edges, we prescribe low-reflection boundary conditions.

We compute the maximum magnitude of the horizontal and vertical components of the displacement field along the red line shown in Fig. 8b, with $10 \leq x_1/\ell \leq 20$. The choice of limiting the evaluation up to a distance of 20ℓ

from the left edge is done to reduce the unavoidable disturbance generated by the reflected wave from the other three sides of the domain. That is because the low-reflection conditions in COMSOL Multiphysics are not able to completely damp out reflections in strongly anisotropic media.

The numerically computed fields $|U_1^0|$ (in grey) and $|U_2^0|$ (in light green) are plotted with thin lines in Fig. 11, as a function of the frequency. A qualitative good agreement is found between the analytical solution of the idealized problem and the numerical one and the mode conversion from longitudinal wave to mixed longitudinal-shear wave can be appreciated in polarization bands.

5 Conclusions

In this work, we employed two-scale asymptotic homogenization to study the propagation of elastic waves in locally resonant metamaterials characterized by a connected stiff matrix and periodically distributed elliptical soft inclusions. This leads to an equivalent homogeneous medium, which has an anisotropic stiffness tensor and an anisotropic frequency-dependent mass tensor.

We discussed how the mass anisotropy influence the dispersion properties of the homogenized medium. In particular, when both principal masses are positive, elastic waves can propagate without attenuation (pass band). If both negative, conversely, only evanescent waves can travel through the medium (band gaps). Furthermore, anisotropy leads to a third case where the principal masses have different signs. In these intervals, called polarization bands, only elastic waves that have a polarization dictated by the metamaterial can propagate without being spatially attenuated.

We investigate the role played by the ellipse eccentricity on the dispersion properties of the homogenized medium, showing how a proper design of the inclusions allows us to obtain different scenarios. In the case of zero eccentricity, only a band gap can be observed. As the eccentricity increases, polarization bands form and the band gap narrows, until only two distinct polarization bands remain in the spectrum.

For the first time in this specific context, we showed that the homogenized formulation, with a frequency dependent anisotropic equivalent mass density, can effectively predict not only the dispersion properties of the infinite metamaterial, but also the wave propagation in a finite system. The solution provided by the homogenized formulation was validated by comparison with the one obtained on the real geometry of the heterogeneous periodic material, finely discretized. The same example allowed us to show that at the opening of the polarization band, the displacement field is polarized along the principal direction of the positive mass. This phenomenon could lead to potential applications where a selective polarization of elastic waves is needed.

Finally, we made use of homogenization to compute an analytical solution in a semi-infinite domain that showed a mode converting mechanism from longitudinal to mixed longitudinal and shear waves in the medium. Numerical simulations on a finite domain showed a satisfactory agreement with the theoretical predictions, thus proving that anisotropic locally-resonant metamaterial can be used to modify the wave mode of propagation.

The homogenization approach here discussed can be employed for an efficient optimization of the material microstructure, opening the way to new design strategies to achieve target properties for elastic wave manipulation.

The effect of geometric imperfections, that break the periodicity of the metamaterial, on polarization band prediction could be investigated by considering quasi-periodic materials with a small modulation parameter, similarly to what has been done in [25] for band gaps. This aspect deserves further research and will be tackled elsewhere.

Author Contributions Conceptualization D.F. and C.C., methodology all authors, analyses and validation D.F., original draft preparation D.F., writing-review-editing all authors, supervision A.V. and C.C.

Funding Open access funding provided by Politecnico di Milano within the CRUI-CARE Agreement.

Data Availability No datasets were generated or analysed during the current study.

Declarations

Conflict of interest The authors have no conflict of interest to declare that are relevant to the content of this article.

References

1. Liu Z, Liu Z, Zhang X, Mao Y, Zhu YY (2000) Locally Resonant Sonic Materials. Science 289(September):1734–1736. https://doi.org/10.1126/science.289.5485.1734
2. D'Alessandro L, Ardito R, Braghin F, Corigliano A (2019) Low frequency 3D ultra-wide vibration attenuation via elastic metamaterial. Sci Rep 9(1):3–10. https://doi.org/10.1038/s41598-019-44507-6
3. Tan KT, Huang HH, Sun CT (2014) Blast-wave impact mitigation using negative effective mass density concept of elastic metamaterials. International Journal of Impact Engineering 64, 20–29 https://doi.org/10.1016/j.ijimpeng.2013.09.003
4. Sugino C, Ruzzene M, Erturk A (2018) Merging mechanical and electromechanical bandgaps in locally resonant metamaterials and metastructures. Journal of the Mechanics and Physics of Solids 116, 323–333 https://doi.org/10.1016/j.jmps.2018.04.005
5. Valappil SV, Aragón AM (2025) Analytical modeling of damped locally-resonant metamaterials. Wave Motion 136:103527
6. Nuland TF, Silva PB, Sridhar A, Geers MG, Kouznetsova VG (2019) Transient analysis of nonlinear locally resonant metamaterials via computational homogenization. Math Mech Solids 24(10):3136–3155
7. Bensoussan A, Lions J-L, Papanicolaou G (1978) Asymptotic Analysis for Periodic Structures. North-Holland Pub. Co., Amsterdam, p 700
8. Auriault JL, Bonnet G (1985) Dynamique des composites élastiques périodiques. Arch.Mech. 37(January 1985), 269–284
9. Craster RV, Kaplunov J, Postnova J (2010) High-frequency asymptotics, homogenisation and localisation for lattices. Q J Mech Appl Math 63(4):497–519. https://doi.org/10.1093/qjmam/hbq015
10. Comi C, Marigo J-J (2020) Homogenization Approach and Bloch-Floquet Theory for Band-Gap Prediction in 2D Locally Resonant Metamaterials. J Elast 139(1):61–90. https://doi.org/10.1007/s10659-019-09743-x
11. Comi C, Moscatelli M, Marigo JJ (2019) Two scale homogenization in ternary locally resonant metamaterials. Mater. Phys. Mech. 44, 8–18 https://doi.org/10.18720/MPM.4412020_2
12. Faraci D, Comi C, Marigo JJ (2022) Band gaps in metamaterial plates: Asymptotic homogenization and bloch–floquet approaches. Journal of Elasticity 148, 55–79 https://doi.org/10.1007/s10659-022-09879-3
13. Park J, Lee D, Rho J (2020) Recent advances in non-traditional elastic wave manipulation by macroscopic artificial structures. Applied Sciences (Switzerland) **10**(2) https://doi.org/10.3390/app10020547
14. Huang Y, Wu JH, Lei Y, Niu J (2023) Impact protection enhancement by negative mass meta-honeycombs with local resonance plates. Composite Structures 321, 117330 https://doi.org/10.1016/j.compstruct.2023.117330
15. Bonnet G, Monchiet V (2022) Negative refraction of elastic waves on a metamaterial with anisotropic local resonance. J Mech Phys Solids 169(May):105060. https://doi.org/10.1016/j.jmps.2022.105060
16. Yang X, Chai Y, Li Y (2021) Metamaterial with anisotropic mass density for full mode-converting transmission of elastic waves in the ultralow frequency range. AIP Advances **11**(12) https://doi.org/10.1063/5.0063038
17. Ma G, Fu C, Wang G, Del Hougne P, Christensen J, Lai Y, Sheng P (2016) Polarization bandgaps and fluid-like elasticity in fully solid elastic metamaterials. Nature Communications 7, 1–8 https://doi.org/10.1038/ncomms13536
18. De Ponti JM, Iorio L, Riva E, Ardito R, Braghin F, Corigliano A (2021) Selective Mode Conversion and Rainbow Trapping via Graded Elastic Waveguides. Phys Rev Appl 16(3):1. https://doi.org/10.1103/PhysRevApplied.16.034028
19. Clement GT, White PJ, Hynynen K (2004) Enhanced ultrasound transmission through the human skull using shear mode conversion. The Journal of the Acoustical Society of America 115(3):1356–1364. https://doi.org/10.1121/1.1645610
20. Jaberzadeh M, Li B, Tan KT (2019) Wave propagation in an elastic metamaterial with anisotropic effective mass density. Wave Motion 89, 131–141 https://doi.org/10.1016/j.wavemoti.2019.03.009

21. Faraci D, Mendicino F, Vincenti A, Comi C (2023) Wave polarization control in anisotropic locally resonant materials. Applied Sciences (Switzerland) **13**(19) https://doi.org/10.3390/app131910797
22. Faraci D, Vincenti A, Comi C (2025) Anisotropic locally resonant metamaterials for elastic waves polarization. In: Proceedings of the 1st Hellenic-Italian Conference on Computational Mechanics, Biomechanics and Mechanics of Materials, Rhodes Island, Greece
23. Yang X, Kweun M, Kim YY (2019) Monolayer metamaterial for full mode-converting transmission of elastic waves. Applied Physics Letters **115**https://doi.org/10.1063/1.5109758
24. Kweun JM, Lee HJ, Oh JH, Seung HM, Kim YY (2017)Transmodal fabry-pérot resonance: Theory and realization with elastic metamaterials. Phys. Rev. Lett. 118, 205901 https://doi.org/10.1103/PhysRevLett.118.205901
25. Moscatelli M, Comi C, Marigo JJ (2024) Wave transmission in quasi-periodic lattices. Philos Trans A Math Phys Eng Sci. **382**https://doi.org/10.1098/rsta.2023.0351

Authors and Affiliations

David Faraci[1] · Angela Vincenti[2] · Claudia Comi[1]

✉ David Faraci
david.faraci@polimi.it

Angela Vincenti
angela.vincenti@sorbonne-universite.fr

Claudia Comi
claudia.comi@polimi.it

[1] Department of Civil and Environmental Engineering, Politecnico di Milano, Piazza Leonardo da Vinci 32, Milan 20133, Italy

[2] Institut Jean Le Rond d'Alembert, Sorbonne Université, CNRS, UMR 7190, F-75005 Paris, France